The Astrophysical Journal Letters, 836:L2 (5pp), 2017 February 10 doi:10.3847/2041-8213/836/1/L2

ALMA [C II] 158 μm Detection of a Redshift 7 Lensed Galaxy behind RX J1347.1−1145*

Maruša Bradač[1], Diego Garcia-Appadoo[2,3], Kuang-Han Huang[1], Livia Vallini[4,5,6], Emily Quinn Finney[1], Austin Hoag[1], Brian C. Lemaux[1], Kasper Borello Schmidt[7], Tommaso Treu[8,18], Chris Carilli[9,10], Mark Dijkstra[11], Andrea Ferrara[12,13], Adriano Fontana[14], Tucker Jones[1], Russell Ryan[15], Jeff Wagg[16], and Anthony H. Gonzalez[17]

[1] Department of Physics, University of California, Davis, CA 95616, USA; marusa@physics.ucdavis.edu
[2] Joint ALMA Observatory, Alonso de Córdova 3107, Vitacura, Santiago, Chile
[3] European Southern Observatory, Alonso de Córdova 3107, Vitacura, Santiago, Chile
[4] Nordita, KTH Royal Institute of Technology and Stockholm University, Roslagstullsbacken 23, SE-106 91 Stockholm, Sweden
[5] Dipartimento di Fisica e Astronomia, viale Berti Pichat 6, I-40127 Bologna, Italy
[6] INAF, Osservatorio Astronomico di Bologna, via Ranzani 1, I-40127 Bologna, Italy
[7] Leibniz-Institut für Astrophysik Potsdam (AIP), An der Sternwarte 16, D-14482 Potsdam, Germany
[8] Department of Physics and Astronomy, UCLA, Los Angeles, CA, 90095-1547, USA
[9] National Radio Astronomy Observatory, P. O. Box 0, Socorro, NM 87801, USA
[10] Cavendish Laboratory, 19 J. J. Thomson Avenue, Cambridge CB3 0HE, UK
[11] Institute of Theoretical Astrophysics, University of Oslo, Postboks 1029 Blindern, NO-0315 Oslo, Norway
[12] Scuola Normale Superiore, Piazza dei Cavalieri 7, I-56126 Pisa, Italy
[13] Kavli IPMU (WPI), Todai Institutes for Advanced Study, The University of Tokyo, Japan
[14] INAF—Osservatorio Astronomico di Roma, Via Frascati 33-00040, Monte Porzio Catone, I-00040 Rome, Italy
[15] Space Telescope Science Institute, 3700 San Martin Drive, Baltimore, MD 21218, USA
[16] Square Kilometre Array Organisation, Lower Withington, Cheshire, UK
[17] Department of Astronomy, University of Florida, 211 Bryant Space Science Center, Gainesville, FL 32611, USA
Received 2016 October 6; revised 2017 January 8; accepted 2017 January 10; published 2017 February 3

Abstract

We present the results of ALMA spectroscopic follow-up of a $z = 6.766$ Lyα emitting galaxy behind the cluster RX J1347.1−1145. We report the detection of [C II] 158 μm line fully consistent with the Lyα redshift and with the peak of the optical emission. Given the magnification of $\mu = 5.0 \pm 0.3$, the intrinsic (corrected for lensing) luminosity of the [C II] line is $L_{[\mathrm{C\,II}]} = 1.4^{+0.2}_{-0.3} \times 10^7\, L_\odot$, roughly ∼5 times fainter than other detections of $z \sim 7$ galaxies. The result indicates that low $L_{[\mathrm{C\,II}]}$ in $z \sim 7$ galaxies compared to the local counterparts might be caused by their low metallicities and/or feedback. The small velocity offset ($\Delta v = 20^{+140}_{-40}$ km s^{-1}) between the Lyα and [C II] line is unusual, and may be indicative of ionizing photons escaping.

Key words: dark ages, reionization, first stars – galaxies: clusters: individual (RX J1347.1−1145) – galaxies: high-redshift – gravitational lensing: strong

1. Introduction

The epoch of reionization, during which the universe became transparent to UV radiation, is still poorly understood. Faint galaxies are likely responsible for this transformation; however this connection is far from confirmed (e.g., Madau & Haardt 2015; Robertson et al. 2015). Despite great progress in finding candidates with *Hubble Space Telescope* (*HST*; e.g., Bouwens et al. 2015) beyond $z \gtrsim 7$, galaxies remain enshrouded in mystery, at least from a spectroscopic point of view. Spectroscopic confirmations remain extremely difficult, as the most prominent spectral feature in the optical/near-IR wavelengths, the Lyα line, can be erased by neutral gas both in and surrounding galaxies.

An alternative way of measuring redshifts for early galaxies is to use sensitive radio/far-infrared (FIR) telescopes to observe the [C II] 158 μm line. It is among the strongest lines in star-forming galaxies at radio through FIR wavelengths (e.g., Carilli & Walter 2013) and it is therefore being actively pursued as a new way to measure redshifts at $z \gtrsim 6$. Furthermore, for lower-redshift galaxies there exists a connection of [C II] to star formation rate (SFR; e.g., De Looze et al. 2014), although for $z \sim 7$ such a relation has not been studied in detail yet due to limited sample size. [C II] is also a very useful tracer of the kinematics of distant galaxies. However, even with ALMA, detections at $z \sim 7$ remain sparse (see Maiolino et al. 2015; Knudsen et al. 2017; Pentericci et al. 2016 for current detections of [C II] and Inoue et al. 2016 for an [O III] 88 μm detection). In particular, despite deep observations, the extremely bright Lyα Emitter (LAE) Himiko was not detected in [C II] (Ouchi et al. 2013; Ota et al. 2014; Schaerer et al. 2015).

From the theoretical side, the issue of non-detections has been studied, e.g., by Vallini et al. (2015), Olsen et al. (2015), and Narayanan & Krumholz (2016). Both Vallini et al. (2015) and Olsen et al. (2015) conclude that in high-z galaxies the [C II] emission arises predominately from photodissociation regions. Furthermore, at $z \sim 7$ the deficit in [C II]-emission at a given SFR has been ascribed to either negative stellar feedback disrupting molecular clouds near the star-forming regions and/or low gas metallicities. Narayanan & Krumholz (2016) point out that the cloud surface density is also a key parameter, with the [C II] luminosity decreasing with decreasing size of the [C II] emitting region in high surface density clouds. Other factors that influence total [C II] emission include (i) the relative abundances of the various gas phases composing the interstellar medium ISM (ionized, neutral, and molecular), (ii)

* These observations are based on the following ALMA data: ADS/JAO. ALMA#2015.1.00091.S. They are also associated with programs *Spitzer* #90009, 60034, 00083, 50610, 03550, 40593, and *HST* # GO10492, GO11591, GO12104, and GO13459. Furthermore based on multi-year KECK programs.
[18] Packard Fellow.

the hardness of the radiation field, and (iii) the temperature and density of the emitting gas.

In this Letter, we report on ALMA observations of RX J1347:1216, a normal ($L < L^*$) star-forming galaxy with Lyα emission at $z_{\rm Ly\alpha} = 6.7659^{+0.0030}_{-0.0005}$. It was first reported by Bradley et al. (2014) and Smit et al. (2014) as a photometrically selected $z \sim 7$ galaxy from the *HST* and *Spitzer* CLASH data (Cluster Lensing And Supernova survey with Hubble; Postman et al. 2012). We have spectroscopically confirmed its redshift using Keck DEIMOS data (Huang et al. 2016) and *HST* grism data from GLASS (Treu et al. 2015; Schmidt et al. 2016). In Huang et al. (2016), we also measured its integrated stellar properties using deep *Spitzer* SURFSUP data (*Spitzer* UltRa Faint SUrvey Program; Bradač et al. 2014). Our magnification model shows that the massive foreground galaxy cluster RX J1347.1−1145 magnifies RX J1347:1216 by a factor fof 5.0 ± 0.3. Taking into account magnification, the galaxy's intrinsic rest-frame UV luminosity is $0.18^{+0.07}_{-0.05}L^*$ (assuming characteristic magnitude at $z \sim 7$ of $M^*_{\rm UV} = -20.87 \pm 0.26$ from Bouwens et al. 2015), making RX J1347:1216 the first galaxy detected with ALMA at $z \sim 7$ having a luminosity characteristic of the majority of galaxies at $z \sim 7$.

Throughout the Letter, we assume a ΛCDM concordance cosmology with $\Omega_{\rm m} = 0.27$, $\Omega_\Lambda = 0.73$, and Hubble constant $H_0 = 73\,{\rm km\,s^{-1}\,Mpc^{-1}}$. Coordinates are given for the epoch J2000.0, and magnitudes are in the AB system.

2. Observations and Data Reduction

We observed RX J1347:1216 with ALMA on 2016 July 21 in Band 6 with 38 12 m antennae on a configuration of 15–700 m baselines. The precipitable water vapor stayed stable at ∼0.8 mm during the observations. The total time on-source was 74 minutes, with the phases centered at the *HST* position of the source. Out of the four spectral windows, SPW0 was set to Frequency Division Mode and its center tuned to the [C II] 158 μm rest-frame frequency of 1900.54 GHz and a sky-frequency of 244.85 GHz, in the Upper Side Band, yielding a velocity resolution of 9.5 km s^{-1} after a spectral averaging factor of 16 was applied to reduce the data rate. The other three spectral windows were used for continuum in Time Division Mode (31.25 MHz spectral resolution) at lower frequencies. We used J1337−1257 for bandpass and absolute flux scale calibrators and J1354−1041 for a phase calibrator.

The data reduction followed the standard procedures in the Common Astronomy Software Applications package. The data cube was cleaned using Briggs weighting and ROBUST = 0.5. The FWHM beam size of the final image is $0\farcs58 \times 0\farcs41$ at a position angle of 288°. The 1σ noise of the [C II] 158 μm line image is $\sigma_{\rm line} = 250\,\mu{\rm Jy\,beam^{-1}}$ at 244.7424 GHz over a channel width of 30 km s^{-1} (24.5 MHz). The continuum image was extracted using all the line-free channels of the four spectral windows, resulting in a continuum sensitivity of <15 μJy (1σ). Flux calibration errors (∼5%) are included in all measurements.

3. Results

We have detected [C II] emission in RX J1347:1216 with Lyα emission first reported by Huang et al. (2016) and Schmidt et al. (2016). The [C II] line is detected at 5σ (peak line flux $S_{\rm line} = 1.25 \pm 0.25$ mJy using 30 km s^{-1} resolution; Figure 1).

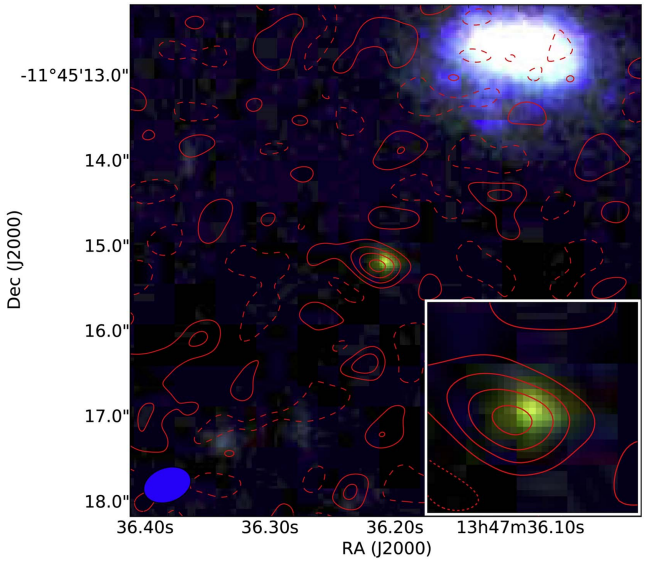

Figure 1. [C II] emission overlaid on the *HST* color composite RGB image (optical-F110W-F160W). The contours are spaced linearly between 1 and 5σ (solid lines); negative contours (-1, -2σ) are given as dashed lines. A $1'' \times 1''$ zoom-in is shown in the inset, and the beam is given in the bottom left.

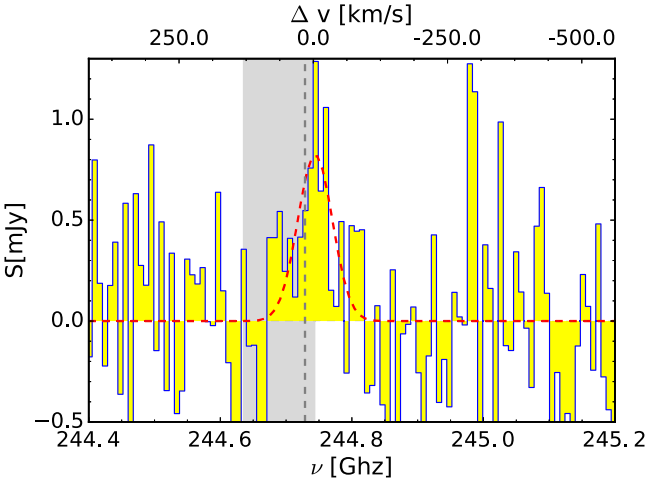

Figure 2. Extracted spectrum (flux S as a function of frequency ν) of the [C II] emission. The red line denotes the best-fit Gaussian (with parameter listed in Table 1) and the gray dashed line and region correspond to the Lyα redshift and uncertainty.

Due to gravitational lensing, we are able to measure [C II] luminosity in RX J1347:1216 that is intrinsically ∼5 times fainter than other such measurements at $z \sim 7$ to date (and similar luminosity to a $z \sim 6$ object in Knudsen et al. 2016). We extract the spectrum using native spectral resolution with a channel width of 9.6 km s^{-1} (7.8125 MHz) and measure [C II] redshift of $z_{\rm [C\,II]} = 6.7655 \pm 0.0005$ (Figure 2). We fit the line using a Gaussian and estimate peak flux of $S_{\rm line,g} = 0.82 \pm 0.26$ mJy, FWHM of 75 ± 25 km s^{-1} and the integrated line flux of $S_{\rm line}\Delta v = 67 \pm 12$ mJy km s^{-1}. The integrated values do not critically depend upon the assumption of a Gaussian profile within the uncertainties. The luminosity is $L_{\rm [C\,ii]} = 1.5^{+0.2}_{-0.4} \times 10^7\,L_\odot$, corrected for lensing and the errors reflect both uncertainties in the flux estimates as well as magnification (Table 1).

We investigate the $L_{\rm [C\,II]}$–SFR connection for this galaxy. The strength of the [C II] emission correlates with the SFR in

Table 1
Stellar Population Modeling Results for RX J1347:1216 using *HST* and *Spitzer* Photometry from Huang et al. (2016), Spectroscopy of Lyα from Keck DEMOS from Huang et al. (2016), and [C II] from ALMA Observations

ALMA	
R.A.	13:47:36.214
Decl.	−11:45:15.20
$z_{[\mathrm{C\,II}]}$	6.7655 ± 0.0005
S_{line}	1.25 ± 0.25 mJy
$S_{\mathrm{line,g}}$ (Gauss Fit)	0.82 ± 0.26 mJy
$S_{\mathrm{line}}\Delta v$(Gauss Fit)	67 ± 12 mJy km s^{-1}
FWHM (Gauss Fit)	75 ± 25 km s^{-1}
$L_{[\mathrm{C\,II}]} \times f_\mu$ [a]	$1.5^{+0.2}_{-0.4} \times 10^7\, L_\odot$
Continuum	<15 μJy (1σ)
$L_{\mathrm{FIR}} \times f_\mu$ [a]	$<2 \times 10^{10}\, L_\odot$ (3σ)
$\mathrm{SFR}_{\mathrm{FIR}} \times f_\mu$ [a]	$<3\, M_\odot$ yr^{-1} (3σ)
HST + *Spitzer* + Keck	
R.A.	13:47:36.207
Decl.	−11:45:15.16
$z_{\mathrm{Ly}\alpha}$	$6.7659^{+0.0030}_{-0.0005}$
$\mathrm{EW}_{\mathrm{Ly}\alpha}$	26 ± 4 Å
$\Delta_{HST-\mathrm{ALMA}}$ [arcsec (kpc)]	0.1 (0.5)
$\Delta v_{\mathrm{Ly}\alpha-[\mathrm{C\,ii}]}$	20^{+140}_{-40} km s^{-1}
F160W [b]	26.1 ± 0.2 mag
μ_0	5.0 ± 0.3
$M_{\mathrm{stellar}} \times f_\mu$ [a]	$8.0^{+6.5}_{-0.9} \times 10^7\, M_\odot$
$\mathrm{SFR}_{\mathrm{SED}} \times f_\mu$ [a]	$8.5^{+5.8}_{-1.0}\, M_\odot$ yr^{-1}
$\mathrm{SFR}_{\mathrm{UV}} \times f_\mu$ [a]	$3.2 \pm 0.4\, M_\odot$ yr^{-1}
Age	$\leqslant$13 Myr
sSFR	$105.1^{+0.1}_{-20}$ Gyr^{-1}
$E(B-V)_{\mathrm{fit}}$	$0.10^{+0.05}_{-0.01}$
β_{UV}	$-2.5^{+0.7}_{-1.0}$

Notes.
[a] The intrinsic properties calculated assuming $\mu = \mu_0$ from this table. To use a different magnification factor μ, simply use $f_\mu \equiv \mu/\mu_0$, i.e., dividing value given in this row by f_μ.
[b] Lensed total magnitude (MAG_AUTO as defined by SExtractor Bertin & Arnouts 1996) in F160W.

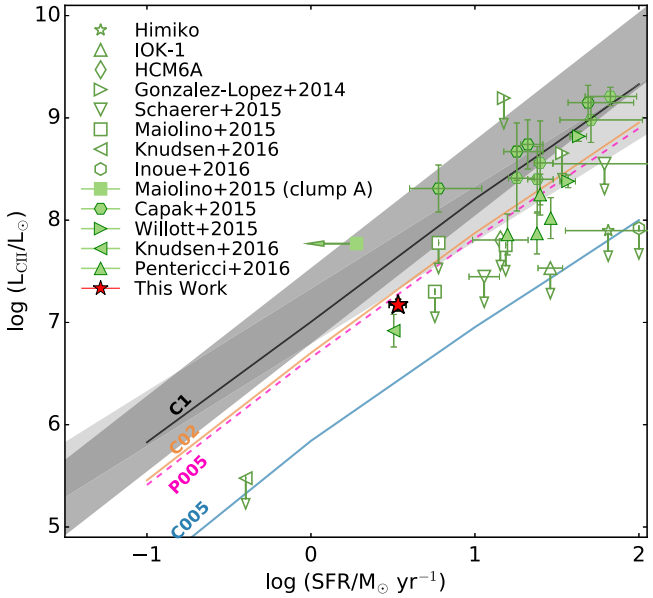

Figure 3. $L_{[\mathrm{C\,II}]}$ vs. SFR at $z > 5$. The red star is the [C II] detection of the object RX J1347:1216; we show the SFR estimated directly from UV luminosity $\mathrm{SFR}_{\mathrm{UV}}$. Lines represent the result from Vallini et al. (2015) obtained assuming a constant metallicity: black for $Z = Z_\odot$ (C1), orange for $Z = 0.2\, Z_\odot$ (C02), and blue for $Z = 0.05\, Z_\odot$ (C005). The magenta dashed line (P005) corresponds to a density-dependent metallicity with $Z = 0.05\, Z_\odot$. The 1σ scatter around the best-fit relations for dwarf and local starburst galaxies from De Looze et al. (2014) are plotted in dark gray and light gray, respectively. The green empty (filled) points represent upper limits (detections) of [C II] in Lyα and Lyman break galaxies at redshifts 5–7 as reported by Pentericci et al. (2016), Knudsen et al. (2016), Inoue et al. (2016), Maiolino et al. (2015), Capak et al. (2015), Willott et al. (2015), Schaerer et al. (2015), González-López et al. (2014), Ota et al. (2014), Ouchi et al. (2013), and Kanekar et al. (2013). We excluded detections in more extreme objects (quasars and starbursts) for the clarity of the plot.

local dwarf galaxies (De Looze et al. 2014); however, the [C II] luminosity is not a simple function of SFR, nor is there a simple correlation between [C II] luminosity and the total mass of the ISM at higher redshifts. This is shown in Figure 3 where we plot $L_{[\mathrm{C\,II}]}$ versus SFR. We include results from simulations by Vallini et al. (2015) as well as results for $z > 5$ galaxies from the literature. We show the SFR of RX J1347:1216 estimated directly from UV luminosity $\mathrm{SFR}_{\mathrm{UV}} = 3.2 \pm 0.4\, M_\odot$ yr^{-1} in Figure 3, assuming no dust attenuation, to compare with values from the literature.

Using ALMA FIR continuum non-detection limits (<15 μJy), we derive $\mathrm{SFR}_{\mathrm{FIR}} < 3\, M_\odot$ yr^{-1} (assuming spectral index $\beta = 1.5$ and conservatively a dust temperature of 45 K). This is in contrast to our nominal SED-fitting results from Huang et al. (2016) using $0.2\, Z_\odot$ templates from Bruzual & Charlot (2003) and assuming Calzetti et al. (2000) dust attenuation curve, which imply a dust-obscured $\mathrm{SFR}_{\mathrm{SED}} \approx 14\, M_\odot$ yr^{-1}, significantly higher than the FIR upper limit. Re-fitting the SED assuming a constant star formation history and a steeper SMC dust attenuation curve (Pei 1992), motivated by recent ALMA results (e.g., Capak et al. 2015), leads to a smaller dust-obscured $\mathrm{SFR}_{\mathrm{SED}} = 5.3\, M_\odot$ yr^{-1}, closer to but still higher than the limit derived from the non-detection of FIR continuum. This is similar to $z \sim 5$ sources in Capak et al. (2015).

The nominal UV slope β_{UV} measured from the observed (i.e., not fitted) F125W to F160W magnitudes (see Huang et al. 2016 for details) is quite blue ($\beta_{\mathrm{UV}} = -2.5^{+0.7}_{-1.0}$) with large uncertainty. The stellar mass is $M_{\mathrm{stellar}} = 8.0^{+6.5}_{-0.9} \times 10^7\, M_\odot$ and young age of $\leqslant$13 Myr (with a maximally old stellar population not contributing >10% of the stellar mass). We list the SED-fitting results using the SMC curve in Table 1 and show the best-fit template in Figure 4. Most of the changes relative to Huang et al. (2016) come from the difference in dust attenuation curve; changing the star formation history alone changes the results by less than 10%.

The low [C II] luminosity given SFR is consistent with models requiring low metallicity $\lesssim 0.2 Z_\odot$, though feedback might play a role as well. As noted by Huang et al. (2016) and Smit et al. (2014), SED modeling for this galaxy (Figure 4) requires strong nebular emission lines to explain its observed IRAC [3.6]–[4.5] color. The object is best fit with a young ($\leqslant$13 Myr) stellar population, low metallicity ($0.2\, Z_\odot$), and strong nebular emission lines (EW > 1000 Å for Hβ and [O III], though note that all these parameters are highly degenerate), giving a consistent picture with lower [C II] luminosity compared to the local galaxies. The recent detection of [O III] 88 μm in a galaxy at $z = 7.2120$ with ALMA by Inoue et al. (2016) along with the upper limit on the [C II] is also in line with our results as it requires very low gas-phase

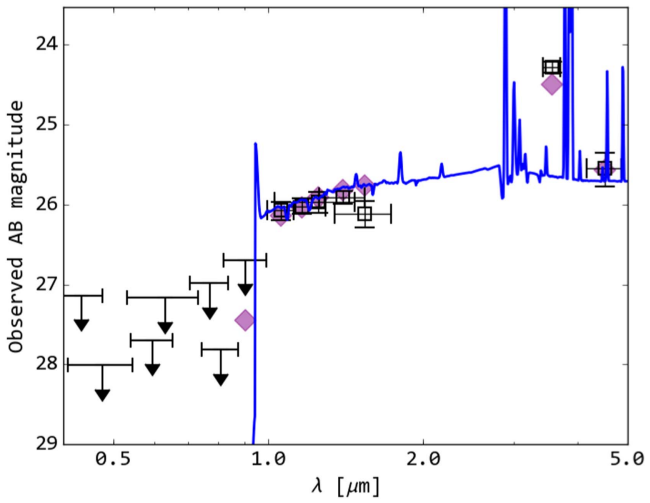

Figure 4. SED fitting of *HST*+*Spitzer* photometry (Huang et al. 2016), using SMC dust attenuation curve from Pei (1992). We assume a metallicity that is $Z = 0.2\,Z_{\odot}$, constant star formation history, and we fix the templates at $z = 6.7655$. Squares/upper limits represent measured photometry from Huang et al. (2016), while purple diamonds indicate the model (blue line) predicted magnitudes in each band.

metallicities (Vallini et al. 2016; see also Cormier et al. 2015 for a study of local dwarf galaxies with high [O III] 88 μm/[C II] ratios).

Following Pentericci et al. (2016) and Wang et al. (2013), we can also estimate the dynamical mass within the [C II]-emitting region of the galaxy. We use $M_{\rm dyn} = 1.16 \times 10^5 V_{\rm cir}^2 D$, where $V_{\rm cir}$ is the circular velocity in km s^{-1}, estimated using $V_{\rm cir} = 0.75 \times {\rm FWHM}_{\rm [CII]}/\sin(i)$, i is the disk inclination angle, and D is the disk diameter in kpc. Note that this approximation is very uncertain, as $z \sim 7$ galaxies might not have ordered motion. However, Pallottini et al. (2017) showed that [C II] mostly arises from an ordered, albeit small, disk. We estimate the disk diameter to be $\sim$0.″6 and obtain $M_{\rm dyn} \sin^2 i = (1.0 \pm 0.5) \times 10^9\,M_{\odot}$. For an intrinsically axisymmetric, infinitesimally thin disk, inclination is related to ellipticity via $\cos i = b/a$, where b/a is the axis ratio. With $b/a = 0.6$ measured from the [C II] emission, we get $i = 50^{\circ}$ and $M_{\rm dyn} = (2.0 \pm 0.9) \times 10^9\,M_{\odot}$ (the error does not include the systematic errors from inclination). This value indicates that $f_{\rm gas} \sim 1 - M^*/M_{\rm dyn} = 96^{+2}_{-10}\%$ of the baryonic mass of this galaxy is in the molecular and atomic gas (contribution of dark matter to $M_{\rm dyn}$ within the [C II]-emitting region is small). The high value is consistent with predictions from the Kennicutt–Schmidt relation of SFR to gas mass (Kennicutt 1998), from which we obtain $M_{\rm gas} = (3.5^{+2.1}_{-1.1}) \times 10^9 M_{\odot}$ (using value ${\rm SFR}_{\rm SED}$ from Table 1).

The [C II] line is spatially consistent (measured offset is 0.″1) with the rest-frame UV emission within the standard ALMA astrometric uncertainty of $\sim$0.″1 (*HST* uncertainty is smaller). In addition, Dunlop et al. (2017) noted that the *HST* and ALMA astrometry of the HUDF presented both a systematic shift of 0.″25 and a random offset of up to 0.″5. Similarly, Pentericci et al. (2016) note 0.″1–0.″6 random offsets measured from serendipitous detections in the field. Unfortunately, we do not detect any other sources in our small field of view to perform relative astrometric calibration.

The Lyα line redshift of this object is also in excellent agreement with the [C II] redshift (Figure 2). The resulting velocity offset of Lyα compared to [C II] is only $\Delta v = 20^{+140}_{-40}$ km s^{-1} (68% confidence, positive Δv indicates that Lyα is redshifted). The Lyα redshift was difficult to determine with a high accuracy given the proximity of a skyline; hence, in Huang et al. (2016), we reported it only with two significant digits. We remeasure the redshift using our DEIMOS data (and improve on absolute wavelength calibration reported in Huang et al. 2016). The reasons for asymmetric errors on the measurement (Table 1) are the proximity of the skyline, lower S/N of the line ($\sim 10\sigma$), and the asymmetric nature of the line. The errors are, however, small, and we do not detect significant shift of the Lyα line.

This is somewhat unexpected, as for such a low-luminosity galaxy ($0.18^{+0.07}_{-0.05} L^*$, rest-frame EW of Lyα 26 ± 4 Å) the outflows are ubiquitous at lower-z. At $z \sim 3$, Erb et al. (2014) reported Lyα velocity shifts of $\Delta v \approx 100$–500 km s^{-1} for low-EW (EW $\lesssim$ 10 Å) LAEs and a strong anti-correlation between Δv and EW. They concluded that Δv is likely modulated both by galaxy continuum luminosity and by Lyα EW. At $z \sim 7$, however, Stark et al. (2015) measured an offset of $\Delta v \approx 60$ km s^{-1} between Lyα and CIV for a lensed low-luminosity galaxy A1703-zd6 at $z = 7.045$ (though CIV might not trace systemic velocity). Pentericci et al. (2016) reported velocity shifts of $\sim$100 km s^{-1} between [C II] and Lyα for their three most significant detections. For a higher-luminosity galaxy, Stark et al. (2017) reported an offset between CIII] and Lyα of $\sim$340 km s^{-1}. Given the small velocity offset of RX J1347:1206 (and similar other low-luminosity galaxies), it seems that at z $\sim$ 7, Lyα is much closer to systemic velocity than is the case for low-z LAEs at similar UV-continuum luminosities.

This is important because velocity offsets are crucial in interpreting the line visibility during the reionization epoch. The low offset is interpreted differently in the so-called shell models versus multi-phase models of LAEs. A shell model requires low neutral gas column density or a high outflow velocity (Verhamme et al. 2015). In the case of a multi-phase model (Dijkstra et al. 2016), a low-velocity offset translates to a low covering fraction of neutral gas, independent of its neutral column density and outflow velocity. In both models, however, the low-velocity offset is a consequence of the presence of low HI-column density escape routes for Lyα photons, which may also allow ionizing photons to escape (see Verhamme et al. 2015, 2017; Dijkstra et al. 2016 for more detailed discussions). For a more general conclusion, a larger sample is needed, but if future observations systematically show smaller velocity offsets, this would imply that the observed drop in LAE fraction between $z \sim 6$ and 7 (e.g., Schenker et al. 2012, 2014; Caruana et al. 2014; Pentericci et al. 2014; Tilvi et al. 2014; Schmidt et al. 2016) is more easily explained by changes in the IGM than in the circumgalactic medium or galactic intrinsic properties (Dijkstra 2014; Choudhury et al. 2015; Mesinger et al. 2015).

4. Conclusions

In this Letter, we report a [C II] ALMA detection of a low-luminosity galaxy at $z = 6.7655$. The [C II] redshift agrees with Lyα redshift and the position agrees with the optical/UV *HST* counterpart of this object (within uncertainties). This indicates that the Lyα is at (or close to) resonant frequency, potentially requiring a lower IGM neutral fraction to explain the drop in the LAE fraction from $z \sim 7$ to $z \sim 6$ if the kinematics of the

Lyα emitting region in RX J1347:1216 are typical of $z \sim 7$ sub-L^* galaxies.

The [C II] luminosity is much lower than that expected from low-redshift low-metallicity dwarf galaxies, yet it is consistent with predictions of simulations of $Z < 0.2\ Z_\odot$ galaxies at $z \sim 7$ by Vallini et al. (2015). The departure of high-z galaxies from local relation is the most likely explanation for why several searches of [C II] emission at $z \sim 7$ have yielded non-detections, as many have assumed the $L_{[\mathrm{C\,II}]}$–SFR relation for local dwarf galaxies (De Looze et al. 2014). Due to gravitational lensing, we reach lower intrinsic flux limits (factor of ∼5) than similar observations of field galaxies, and as a result we are able to study a source that belongs to the bulk of the population at $z \sim 7$. As shown in this study, such lens-magnified observations enable studies of the ISM in the sources responsible for reionization. Future high-resolution observations with ALMA will allow us to resolve (spectrally and spatially) more galaxies at $z \sim 7$ and study in detail the kinematics and spatial distributions of [C II]-emitting gas at sub-kiloparsec scales. Such studies will firmly establish ALMA as the premiere facility that will revolutionize the explorations of the earliest galaxies and our understanding of their place in the galaxy evolution and reionization puzzle.

We would like to thank Sergio Martin for help with the ALMA data. The work was carried out by M.B. while visiting Joint ALMA Observatory (JAO); M.B. acknowledges support for the visit by JAO through ALMA visitor program. This Letter makes use of the following ALMA data: ADS/JAO. ALMA#2015.1.00091.S. ALMA is a partnership of ESO (representing its member states), NSF (USA) and NINS (Japan), together with NRC (Canada), NSC and ASIAA (Taiwan), and KASI (Republic of Korea), in cooperation with the Republic of Chile. The Joint ALMA Observatory is operated by ESO, AUI/NRAO and NAOJ. Support was provided by NRAO via the NRAO Student Observing Support (SOS) Program. This material is based upon work supported by Associated Universities, Inc./National Radio Astronomy Observatory and the National Science Foundation Observations were also carried out using *Spitzer* Space Telescope, which is operated by the Jet Propulsion Laboratory, California Institute of Technology under a contract with NASA. Also based on observations made with the NASA/ESA *Hubble Space Telescope*, obtained at the Space Telescope Science Institute, which is operated by the Association of Universities for Research in Astronomy, Inc., under NASA contract NAS 5-26555 and NNX08AD79G and W.M. Keck Observatory, which is operated as a scientific partnership among the California Institute of Technology, the University of California and the National Aeronautics and Space Administration. The Observatory was made possible by the generous financial support of the W.M. Keck Foundation. Support for this work was provided by NASA through an award issued by JPL/Caltech and through *HST*-AR-13235, *HST*-GO-13459, *HST*-GO-13177, *HST*-GO-10200, *HST*-GO-10863, and *HST*-GO-11099 from STScI. T.T. acknowledges support by the Packard Fellowship. A.H. acknowledges support by NASA Headquarters under the NASA Earth and Space Science Fellowship Program Grant ASTRO14F-0007. The authors wish to recognize and acknowledge the very significant cultural role and reverence that the summit of Mauna Kea has always had within the indigenous Hawaiian community. We are most fortunate to have the opportunity to conduct observations from this mountain.

Facilities: ALMA, *Spitzer* (IRAC), *HST* (ACS/WFC3), Keck:Deimos.

References

Bertin, E., & Arnouts, S. 1996, A&AS, 117, 393
Bouwens, R. J., Illingworth, G. D., Oesch, P. A., et al. 2015, ApJ, 803, 34
Bradač, M., Ryan, R., Casertano, S., et al. 2014, ApJ, 785, 108
Bradley, L. D., Zitrin, A., Coe, D., et al. 2014, ApJ, 792, 76
Bruzual, G., & Charlot, S. 2003, MNRAS, 344, 1000
Calzetti, D., Armus, L., Bohlin, R. C., et al. 2000, ApJ, 533, 682
Capak, P. L., Carilli, C., Jones, G., et al. 2015, Natur, 522, 455
Carilli, C., & Walter, F. 2013, ARA&A, 51, 105
Caruana, J., Bunker, A. J., Wilkins, S. M., et al. 2014, MNRAS, 443, 2831
Choudhury, T. R., Puchwein, E., Haehnelt, M. G., & Bolton, J. S. 2015, MNRAS, 452, 261
Cormier, D., Madden, S. C., Lebouteiller, V., et al. 2015, A&A, 578, A53
De Looze, I., Cormier, D., Lebouteiller, V., et al. 2014, A&A, 568, A62
Dijkstra, M. 2014, PASA, 31, e040
Dijkstra, M., Gronke, M., & Venkatesan, A. 2016, ApJ, 828, 71
Dunlop, J. S., McLure, R. J., Biggs, A. D., et al. 2017, MNRAS, 466, 861
Erb, D. K., Steidel, C. C., Trainor, R. F., et al. 2014, ApJ, 795, 33
González-López, J., Riechers, D. A., Decarli, R., et al. 2014, ApJ, 784, 99
Huang, K.-H., Bradač, M., Lemaux, B. C., et al. 2016, ApJ, 817, 11
Inoue, A. K., Tamura, Y., Matsuo, H., et al. 2016, Sci, 352, 1559
Kanekar, N., Wagg, J., Ram Chary, R., & Carilli, C. L. 2013, ApJL, 771, L20
Kennicutt, R. C., Jr. 1998, ApJ, 498, 541
Knudsen, K. K., Richard, J., Kneib, J.-P., et al. 2016, MNRAS, 462, L6
Knudsen, K. K., Watson, D., Frayer, D., et al. 2017, MNRAS, 466, 138
Madau, P., & Haardt, F. 2015, ApJL, 813, L8
Maiolino, R., Carniani, S., Fontana, A., et al. 2015, MNRAS, 452, 54
Mesinger, A., Aykutalp, A., Vanzella, E., et al. 2015, MNRAS, 446, 566
Narayanan, D., & Krumholz, M. 2016, MNRAS, submitted (arXiv:1601.05803)
Olsen, K. P., Greve, T. R., Narayanan, D., et al. 2015, ApJ, 814, 76
Ota, K., Walter, F., Ohta, K., et al. 2014, ApJ, 792, 34
Ouchi, M., Ellis, R., Ono, Y., et al. 2013, ApJ, 778, 102
Pallottini, A., Ferrara, A., Gallerani, S., et al. 2017, MNRAS, 465, 2540
Pei, Y. C. 1992, ApJ, 395, 130
Pentericci, L., Carniani, S., Castellano, M., et al. 2016, ApJL, 829, L11
Pentericci, L., Vanzella, E., Fontana, A., et al. 2014, ApJ, 793, 113
Postman, M., Coe, D., Benítez, N., et al. 2012, ApJS, 199, 25
Robertson, B. E., Ellis, R. S., Furlanetto, S. R., & Dunlop, J. S. 2015, ApJL, 802, L19
Schaerer, D., Boone, F., Zamojski, M., et al. 2015, A&A, 574, A19
Schenker, M. A., Ellis, R. S., Konidaris, N. P., & Stark, D. P. 2014, ApJ, 795, 20
Schenker, M. A., Stark, D. P., Ellis, R. S., et al. 2012, ApJ, 744, 179
Schmidt, K. B., Treu, T., Bradač, M., et al. 2016, ApJ, 818, 38
Smit, R., Bouwens, R. J., Labbé, I., et al. 2014, ApJ, 784, 58
Stark, D. P., Ellis, R. S., Charlot, S., et al. 2017, MNRAS, 464, 469
Stark, D. P., Walth, G., Charlot, S., et al. 2015, MNRAS, 454, 1393
Tilvi, V., Papovich, C., Finkelstein, S. L., et al. 2014, ApJ, 794, 5
Treu, T., Schmidt, K. B., Brammer, G. B., et al. 2015, ApJ, 812, 114
Vallini, L., Ferrara, A., Pallottini, A., & Gallerani, S. 2016, MNRAS, in press (arXiv:1606.08464)
Vallini, L., Gallerani, S., Ferrara, A., Pallottini, A., & Yue, B. 2015, ApJ, 813, 36
Verhamme, A., Orlitova, I., Schaerer, D., et al. 2017, A&A, 597, A13
Verhamme, A., Orlitová, I., Schaerer, D., & Hayes, M. 2015, A&A, 578, A7
Wang, R., Wagg, J., Carilli, C. L., et al. 2013, ApJ, 773, 44
Willott, C. J., Carilli, C. L., Wagg, J., & Wang, R. 2015, ApJ, 807, 180